AAS 17-291

CONSTRAINED LOW-THRUST SATELLITE FORMATION-FLYING USING RELATIVE ORBIT ELEMENTS

Lukas M. Steindorf[*], Simone D'Amico[†], Julian Scharnagl[‡], Florian Kempf[§], and Klaus Schilling[¶]

This paper proposes a continuous low-thrust guidance and control strategy for constrained satellite formation-flying in perturbed orbits of arbitrary eccentricity. The controller feeds back mean relative orbit elements (ROE) and is based on Lyapunov theory. A novel feedback gain matrix, which enables the spacecraft to autonomously apply thrust at fuel efficient locations is presented. The guidance strategy makes use of a reference governor, which is designed in ROE state-space in order to ensure that all constraints imposed on the formation-flying mission are satisfied. The reference governor can enforce wall, thrust and time constraints. To achieve near-optimal fuel consumption, an autonomous algorithm to leverage Keplerian dynamics is developed. Orbit perturbations include the differential Earth oblateness effect J_2 and aerodynamic drag. The control and guidance strategy is developed for the nanosatellite formation-flying mission NetSat, which is developed by the Zentrum für Telematik e.V. NetSat will launch four identical spacecraft into a low Earth orbit to demonstrate fully autonomous guidance, navigation and control with low-thrust electrical propulsion.

INTRODUCTION

Low-thrust guidance and control of the relative motion between multiple spacecraft is a field of study with increasing importance, as future formation-flying missions follow the miniaturization trend of spacecraft. Particularly, strategies for relative position control must address limited thrusting and propellant capabilities while maintaining operational aspects, such as collision safety and time constraints. One such mission is NetSat,[1] a nanosatellite (cubesat) formation mission created by the Zentrum für Telematik e.V., which intends to prove the feasibility to operate a formation of four spacecraft as an enabling technology for scientific experiments, as well as commercial applications. The formation consists of four identical and maneuverable spacecraft, which are equipped with a field emission electrical propulsion system (NanoFEEP)[2] developed by the Universities of Dresden and Würzburg. The propulsion system provides thrust levels ranging from $0.24\,\mu$N up to $77.8\,\mu$N to accelerate spacecraft with a mass of $1.3\,$kg.

Several low-thrust formation control strategies have been described in the available body of literature. Schaub et al.[3] proposed a feedback law based on mean classical orbit elements. A feedback

[*]Research Scholar, Stanford University, Dept. of Aeronautics and Astronautics, Space Rendezvous Laboratory, Durand Building, 496 Lomita Mall, Stanford, CA 94305-4035
[†]Assistant Professor, Stanford University, Dept. of Aeronautics and Astronautics, Space Rendezvous Laboratory, Durand Building, 496 Lomita Mall, Stanford, CA 94305-4035
[‡]Doctoral Candidate, Zentrum für Telematik, Magdalene-Schoch-Straße 5, 97074 Würzburg, Germany
[§]Doctoral Candidate, University of Würzburg, Dept. of Computer Sciences, Am Hubland, 97074 Würzburg, Germany
[¶]Professor, University of Würzburg, Dept. of Computer Sciences, Am Hubland, 97074 Würzburg, Germany

gain matrix inspired by Gauss' variational equations[4] is designed to efficiently control each mean orbit element at a fuel-optimal location in orbit. However, combining maneuvers can yield significant delta-v savings. Furthermore, the controller is designed for J_2-invariant relative orbits only. Guelman and Aleshin,[5] Lembeck and Prussing,[6] and Carter[7] utilize optimum control theory on relative position and velocity. While optimum control allows to enforce lower and upper bounds of the control inputs, a disadvantage of optimal control theory is the fact that a set of nonlinear differential equations has to be solved on-board of small spacecraft with limited computational power. A common difficulty of controlling relative position and velocity is the inclusion of orbit perturbations in the plant and state transition matrices. Dunbar and Murray[8] formulate a nonlinear, constrained model predictive control problem and provide conditions for closed-loop stability. The main drawback is again that no analytical solution exists. The adaptive continuous controller of de Queiroz et al.[9] uses a full state feedback to control relative position tracking error. The issue is that the unknown spacecraft masses and perturbation forces are assumed to be constant and the restriction to circular orbits.

This paper presents a guidance and control strategy for small satellites with low-thrust levels in low Earth orbit (LEO) aiming to achieve arbitrary formation reconfigurations and satisfying a constraint set, while minimizing collision risk and system complexity. The goals are to guide the spacecraft on fuel-efficient trajectories and to autonomously center the continuous control maneuvers at the optimal location in orbit. In order to decrease the demands on the attitude control system, thrust vectors are only applied into the flight direction and normal to the orbit plane. The control law is based on Lyapunov theory combined with mean relative orbit element (ROE)[10] state feedback with an innovative feedback gain matrix, which is inspired by the fuel-optimal impulsive approach[11] to formation control. Thus, the computational efforts are kept at a minimum and allow on-board execution. Using mean ROE allows to use plant matrices that include secular and periodic perturbations, such as the Earth's oblateness effect and differential drag.[12,13] Moreover, the minimum delta-v problem can be translated into a minimum path-planning problem in ROE space.[11,14] The proposed control strategy leverages Keplerian dynamics to increase delta-v efficiency and reduce system complexity. The guidance solution is based on potential fields and a technique to re-formulate all constraints that are imposed on the relative state as one single constraint. This is achieved by designing a reference governor[15–17] in ROE space. Constraint types, which are investigated in this study, are a time constraint, a thrust level constraint, wall constraints and a passive collision avoidance constraint. All presented algorithms are applicable to closed reference orbits of arbitrary eccentricity.

MEAN RELATIVE ORBIT ELEMENTS AND RELATIVE SATELLITE MOTION

The relative motion is described by quasi non-singular ROE,[10] which are nonlinear combinations of the mean classical Keplerian elements a, e, i, ω, Ω and M of the chief and deputy spacecraft

$$\delta\bar{\boldsymbol{\alpha}} = \begin{pmatrix} \delta a \\ \delta\lambda \\ \delta e_x \\ \delta e_y \\ \delta i_x \\ \delta i_y \end{pmatrix} = \begin{pmatrix} \delta a \\ \delta\lambda \\ \delta e\cos\sigma \\ \delta e\sin\sigma \\ \delta i\cos\theta \\ \delta i\sin\theta \end{pmatrix} = \begin{pmatrix} (a-a_c)/a_c \\ \varphi-\varphi_c+(\Omega-\Omega_c)\cos i_c \\ e\cos\omega - e_c\cos\omega_c \\ e\sin\omega - e_c\sin\omega_c \\ i-i_c \\ (\Omega-\Omega_c)\sin i_c \end{pmatrix} , \tag{1}$$

where $\varphi = \omega + M$ is the mean argument of latitude. The subscript c refers to the chief spacecraft, which defines the origin of the **RTN** orbital frame (**R** pointing along the orbit's radius, **N** pointing

along the angular momentum vector, and $\mathbf{T} = \mathbf{N} \times \mathbf{R}$ pointing into the direction of motion for a circular orbit). The quantities δa, $\delta\lambda$, $\delta\boldsymbol{e} = (\delta e_x, \delta e_y)^{\mathrm{T}}$ and $\delta\boldsymbol{i} = (\delta i_x, \delta i_y)^{\mathrm{T}}$ represent the relative semi-major axis, the relative mean longitude, and the relative eccentricity and inclination vectors, respectively. The phases of the relative eccentricity/inclination vectors are named relative perigee σ and relative ascending node θ. Throughout this paper $\delta(.)$ denotes a ROE vector element and $\Delta(.)$ an arithmetic difference. ROE provide intuitive insight into the relative motion in the **RTN** orbital frame. The amplitudes of the relative motion are given by $a_c\|\delta\boldsymbol{e}\|$ in radial ($\boldsymbol{R}$) direction, $2a_c\|\delta\boldsymbol{e}\|$ in along-track ($\boldsymbol{T}$) direction and $a_c\|\delta\boldsymbol{i}\|$ in normal ($\boldsymbol{N}$) direction. Offsets in along-track and radial directions are given by $a_c\delta\lambda$ and $a_c\delta a$, respectively.[18] For elliptic orbits this motion is superimposed by an additional mode at twice the frequency and an amplitude, which is proportional to the eccentricity e_c of the chief spacecraft.[11]

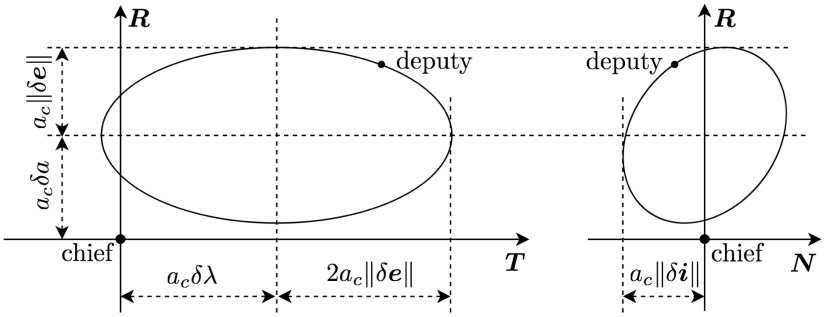

Figure 1: Relative motion of two spacecraft: in-plane motion (left) and out-of-plane motion (right) illustrated in the RTN orbital frame. Note that the relative motion is osculating due to orbit perturbations and no drift is shown for simplicity.

LINEAR DYNAMIC MODEL

The full state-space model consists of three control inputs and seven outputs. The input vector is $\bar{\boldsymbol{u}} = (u_r, u_t, u_n)^{\mathrm{T}}$, which are the control accelerations into radial, tangential and normal direction of the **RTN** orbital frame, respectively. The output is the ROE vector $\delta\bar{\boldsymbol{\alpha}}$ augmented with the time derivative of the relative semi-major axis $\delta\dot{a}$ in order to account for differential drag. The state-space model is given by

$$\begin{bmatrix} \delta\dot{\bar{\boldsymbol{\alpha}}} \\ \delta\ddot{a} \end{bmatrix} = \bar{\boldsymbol{A}}_c \begin{bmatrix} \delta\bar{\boldsymbol{\alpha}} \\ \delta\dot{a} \end{bmatrix} + \begin{bmatrix} \bar{\boldsymbol{B}}_c \\ \mathbf{0}^{1x3} \end{bmatrix} \bar{\boldsymbol{u}} \quad . \tag{2}$$

The plant matrix $\bar{\boldsymbol{A}}_c = \bar{\boldsymbol{A}}_{J_2} + \bar{\boldsymbol{A}}_{\text{drag}} + \bar{\boldsymbol{A}}_{\text{K}}$ takes into account the differential Earth oblateness effect $\bar{\boldsymbol{A}}_{J_2}$, differential drag $\bar{\boldsymbol{A}}_{\text{drag}}$ and Keplerian motion $\bar{\boldsymbol{A}}_{\text{K}}$, which are derived by Koenig et al.[13] The complete plant matrix for the augmented state is given by

$$\bar{\boldsymbol{A}}_c = \kappa \begin{bmatrix} 0 & 0 & 0 & 0 & 0 & 0 & 1/\kappa \\ -\frac{7}{2}EP - \frac{3}{2}\frac{n_c}{\kappa} & 0 & e_xGFP & e_yGFP & -FS & 0 & 0 \\ \frac{7}{2}e_yQ & 0 & -(4e_xe_yG + C)Q & -(1 + 4e_y^2G - D)Q & 5e_yS & 0 & \frac{D-e_x}{\kappa} \\ -\frac{7}{2}e_xQ & 0 & (1 + 4e_x^2G - D)Q & (4e_xe_yG - C)Q & -5e_xS & 0 & \frac{C-e_y}{\kappa} \\ 0 & 0 & 0 & 0 & 0 & 0 & 0 \\ \frac{7}{2}S & 0 & -4e_xGS & -4e_yGS & 2T & 0 & 0 \\ 0 & 0 & 0 & 0 & 0 & 0 & 0 \end{bmatrix}, \tag{3}$$

where n_c is the mean motion. The parameters of the plant matrix are given by[13]

$$\gamma = \frac{3}{4} J_2 R_e^2 \sqrt{\mu}, \qquad \eta_c = \sqrt{1-e_c^2}, \qquad \kappa = \frac{\gamma}{a_c^{7/2}\eta_c^4}, \qquad e_x = e_c \cos\omega_c, \qquad e_y = e_c \sin\omega_c,$$

$$C = \sin\omega_c, \qquad D = \cos\omega_c, \qquad E = 1+\eta_c, \qquad F = 4+3\eta_c, \qquad G = \frac{1}{\eta_c^2},$$

$$P = 3\cos(i_c)^2 - 1, \qquad Q = 5\cos(i_c)^2 - 1, \qquad S = \sin(2i_c), \qquad T = \sin(i_c)^2.$$

In order to account for differential drag, the density-model-free formulation by Koenig et al.[13] is implemented into $\bar{\boldsymbol{A}}_c$. It is essential to properly initialize $\delta\dot{a}$ by in-situ measurements of $\delta\dot{a}_{\text{drag}}$ by tracking the difference over a few orbits without any applied maneuvers during that time. The control input matrix $\bar{\boldsymbol{B}}_c \in \mathbb{R}^{6x3}$ is given by[11]

$$\bar{\boldsymbol{B}}_c = \frac{1}{a_c n_c} \begin{bmatrix} \frac{2}{\eta_c} e_c \sin f_c & \frac{2}{\eta_c}(1+e_c\cos f_c) & 0 \\ -\frac{2\eta_c^2}{1+e_c\cos f_c} & 0 & 0 \\ \eta_c \sin(\omega_c+f_c) & \eta_c \frac{(2+e_c\cos f_c)\cos(\omega_c+f_c)+e_x}{1+e_c\cos f_c} & \frac{\eta_c e_y}{\tan i_c}\frac{\sin(\omega_c+f_c)}{1+e_c\cos f_c} \\ -\eta_c \cos(\omega_c+f_c) & \eta_c \frac{(2+e_c\cos f_c)\sin(\omega_c+f_c)+e_y}{1+e_c\cos f_c} & \frac{-\eta_c e_x}{\tan i_c}\frac{\sin(\omega_c+f_c)}{1+e_c\cos f_c} \\ 0 & 0 & \eta_c \frac{\cos(\omega_c+f_c)}{1+e_c\cos f_c} \\ 0 & 0 & \eta_c \frac{\sin(\omega_c+f_c)}{1+e_c\cos f_c} \end{bmatrix}, \tag{4}$$

where f_c is the true anomaly. The study of the control input matrix $\bar{\boldsymbol{B}}_c$ shows that changes of the relative eccentricity vector $\delta\boldsymbol{e}$ and the relative semi-major axis δa are most efficiently achieved by applying tangential thrust only. This suggests to control the system given by Equation (2) without radial thrust. Furthermore, the delta-v lower bound for impulsive maneuvering is yielded using tangential thrust only for in-plane reconfigurations.[11,19] On the other hand, $\delta\lambda$ can only be controlled directly by radial thrust and therefore waiving radial thrust would mean the loss of full controllability. In this situation, it is convenient to use a reduced model and to control $\delta\dot{\lambda}$ by leveraging Keplerian dynamics. De Florio et al.[20] implement this leverage by augmenting the state with $\delta\dot{\lambda}$ and a proper in-orbit placement of the impulsive along-track maneuvers. A different method, presented in this paper, is to change the applied reference of the relative semi-major axis that will then be followed by a stabilizing feedback controller to maintain full controllability of the complete ROE set $\delta\bar{\boldsymbol{\alpha}}$. Note that in this paper all variables related to the full state are denoted by a bar and variables related to the reduced model are defined without a bar.

REDUCED MODEL

The reduced model does not contain the mean along-track separation as given by the relative mean longitude $\delta\lambda$ such that the reduced ROE vector is defined as $\delta\boldsymbol{\alpha} = (\delta a, \delta e_x, \delta e_y, \delta i_x, \delta i_y)^{\mathrm{T}}$. Furthermore, the control input for the reduced model is defined by the accelerations in along-track and normal direction of the **RTN** orbital frame $\boldsymbol{u} = (u_t, u_n)^{\mathrm{T}}$. The reduced model is given by

$$\begin{bmatrix} \delta\dot{\boldsymbol{\alpha}} \\ \delta\ddot{a} \end{bmatrix} = \boldsymbol{A}_c \begin{bmatrix} \delta\boldsymbol{\alpha} \\ \delta\dot{a} \end{bmatrix} + \begin{bmatrix} \boldsymbol{B}_c \\ \boldsymbol{0}^{1x2} \end{bmatrix} \boldsymbol{u} \quad . \tag{5}$$

The reduced plant matrix is given by

$$\boldsymbol{A}_c = \kappa \begin{bmatrix} 0 & 0 & 0 & 0 & 0 & 1/\kappa \\ \frac{7}{2}e_y Q & -(4e_x e_y G + C)Q & -(1+4e_y^2 G - D)Q & 5e_y S & 0 & \frac{D-e_x}{\kappa} \\ -\frac{7}{2}e_x Q & (1+4e_x^2 G - D)Q & (4e_x e_y G - C)Q & -5e_x S & 0 & \frac{C-e_y}{\kappa} \\ 0 & 0 & 0 & 0 & 0 & 0 \\ \frac{7}{2}S & -4e_x GS & -4e_y GS & 2T & 0 & 0 \\ 0 & 0 & 0 & 0 & 0 & 0 \end{bmatrix} \quad , \tag{6}$$

where the parameters are the same as for Equation (6). Note that Keplerian dynamics have no influence on $\delta\boldsymbol{\alpha}$. The reduced control input matrix is

$$\boldsymbol{B}_c = \frac{1}{a_c n_c} \begin{bmatrix} \frac{2}{\eta_c}(1 + e_c \cos f_c) & 0 \\ \eta_c \frac{(2+e_c \cos f_c)\cos(\omega_c + f_c) + e_x}{1 + e \cos f_c} & \frac{\eta_c e_y}{\tan i_c} \frac{\sin(\omega_c + f_c)}{1 + e_c \cos f_c} \\ \eta_c \frac{(2+e_c \cos f_c)\sin(\omega_c + f_c) + e_y}{1 + e_c \cos f_c} & \frac{-\eta_c e_x}{\tan i_c} \frac{\sin(\omega_c + f_c)}{1 + e_c \cos f_c} \\ 0 & \eta_c \frac{\cos(\omega_c + f_c)}{1 + e_c \cos f_c} \\ 0 & \eta_c \frac{\sin(\omega_c + f_c)}{1 + e_c \cos f_c} \end{bmatrix} \quad . \tag{7}$$

CONTROL STRATEGY

Stabilizing feedback

The feedback controller has to stabilize the system at an applied reference $\delta\boldsymbol{\alpha}_a$. A control law which ensures the relative spacecraft state to asymptotically tend to the applied reference is given by

$$\boldsymbol{u} = -\boldsymbol{B}^{\star}\left[\boldsymbol{A}\delta\boldsymbol{\alpha} + \boldsymbol{P}\Delta\delta\boldsymbol{\alpha}\right] \quad , \tag{8}$$

with $\Delta\delta\boldsymbol{\alpha} = \delta\boldsymbol{\alpha} - \delta\boldsymbol{\alpha}_a$ and $(.)^{\star}$ denoting the pseudo inverse. Let the system described by Equation (5) be subject to the control law given in (8) with $\boldsymbol{P}$ being positive definite. A Lyapunov function candidate is given by

$$V = \frac{1}{2}\Delta\delta\boldsymbol{\alpha}^{\mathrm{T}}\Delta\delta\boldsymbol{\alpha} \quad . \tag{9}$$

If the derivative of Equation (9) is negative definite one can proof that Equation (9) is a Lyapunov function. The derivative is derived by

$$\begin{aligned} \dot{V} &= \Delta\delta\boldsymbol{\alpha}^{\mathrm{T}}\Delta\delta\dot{\boldsymbol{\alpha}} = \Delta\delta\boldsymbol{\alpha}^{\mathrm{T}}\left(\delta\dot{\boldsymbol{\alpha}} - \delta\dot{\boldsymbol{\alpha}}_a\right) = \Delta\delta\boldsymbol{\alpha}\left(\boldsymbol{A}\delta\boldsymbol{\alpha} + \boldsymbol{B}\left(-\boldsymbol{B}^{\star}\left[\boldsymbol{A}\delta\boldsymbol{\alpha} + \boldsymbol{P}\Delta\delta\boldsymbol{\alpha}\right]\right)\right) \quad , \\ &= -\Delta\delta\boldsymbol{\alpha}^{\mathrm{T}}\boldsymbol{P}\Delta\delta\boldsymbol{\alpha} \quad , \end{aligned} \tag{10}$$

which is negative definite. In order to improve fuel efficiency, the Lyapunov feedback gain matrix $\boldsymbol{P}$ is designed such that it determines delta-v efficient locations to apply control inputs

$$\boldsymbol{P} = \frac{1}{k}\begin{pmatrix} \cos(J)^N & 0 & 0 & 0 & 0 \\ 0 & \cos(J)^N & 0 & 0 & 0 \\ 0 & 0 & \cos(J)^N & 0 & 0 \\ 0 & 0 & 0 & \cos(H)^N & 0 \\ 0 & 0 & 0 & 0 & \cos(H)^N \end{pmatrix} \quad , \tag{11}$$

where $k \in \mathbb{R}^+$ is an arbitrary large scaling scalar, $J = \varphi - \bar{\varphi}_{ip}$ and $H = \varphi - \bar{\varphi}_{oop}$. The exponent $N \in \mathbb{N} | N \bmod 2 = 0 \wedge N \geq 2$ defines to which extent the control inputs are centered around the

fuel optimal locations to control the in-plane (δa, $\delta \boldsymbol{e}$) motion at $\bar{\varphi}_{ip}$ and the out-of-plane ($\delta \boldsymbol{i}$) motion at $\bar{\varphi}_{oop}$. The optimal locations for near-circular orbits to apply thrust are given by[11]

$$\bar{\varphi}_{ip} = \text{atan2}\left(\frac{\Delta\delta e_y}{\Delta\delta e_x}\right) \quad , \tag{12}$$

$$\bar{\varphi}_{oop} = \text{atan2}\left(\frac{\Delta\delta i_y}{\Delta\delta i_x}\right) \quad , \tag{13}$$

in the case of a dominant variation of the eccentricity vector ($\Delta\delta e \gg \Delta\delta a$), which is true for bounded motion. The more complex solution for optimal maneuver locations in eccentric reference orbits is given by Chernick and D'Amico.[11] Fuel balancing between the spacecraft pair is achieved by keeping the spacecraft attitudes constant, with their thrusters aligned in positive flight and normal orbit direction. If the control law given in Equation (8) yields a positive control input it is executed by the deputy spacecraft, whereas a negative control input is executed by the chief spacecraft.

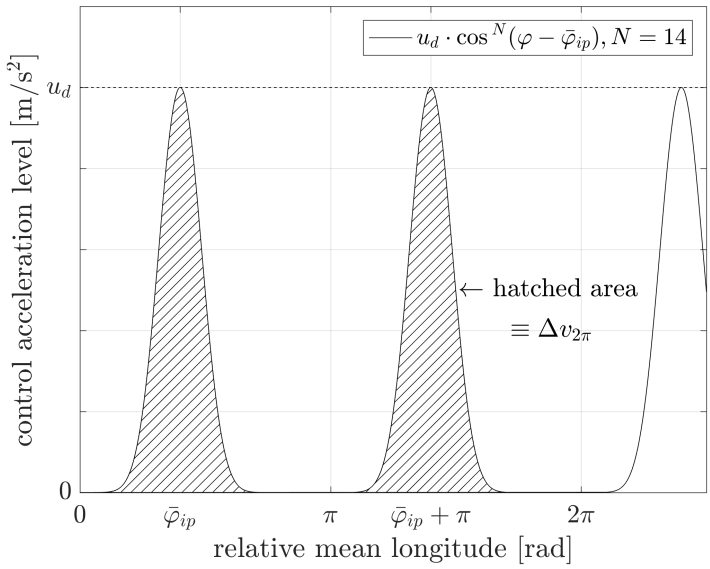

Figure 2: Control inputs of the form $u_d \cdot \cos^N(\varphi - \bar{\varphi}_{ip})$ as shaped by the feedback gain matrix $\boldsymbol{P}$. Here shown for $N = 14$ and a random fuel optimal relative mean latitude $\bar{\varphi}_{ip}$. The hatched area represents the delta-v that is applied during one complete orbit period.

Controlling the Relative Mean Longitude

The relative mean longitude (or the along-track separation) $\delta\lambda$ can only be directly controlled via thrust into the radial direction of the **RTN** frame. Yet, if for the reason of fuel efficiency no radial thrust is to be applied, it can be indirectly controlled by leveraging natural (Keplerian) orbit dynamics

$$\delta\dot{\lambda} = -\frac{3}{2} n_c \cdot \delta a \quad . \tag{14}$$

A change of the relative semi-major axis is effectively achieved by applying tangential thrust (see Equation (4)). Once a difference in the semi-major axes is established, both satellites will drift towards or away from each other in along-track direction. The desired change of $\delta\lambda$ is then only a

matter of time and not a matter of fuel any longer. When the error of the relative mean longitude $\Delta\delta\lambda$ becomes zero also the desired along-track drift $\delta\dot{\lambda}_{\text{a}}$ should become zero.

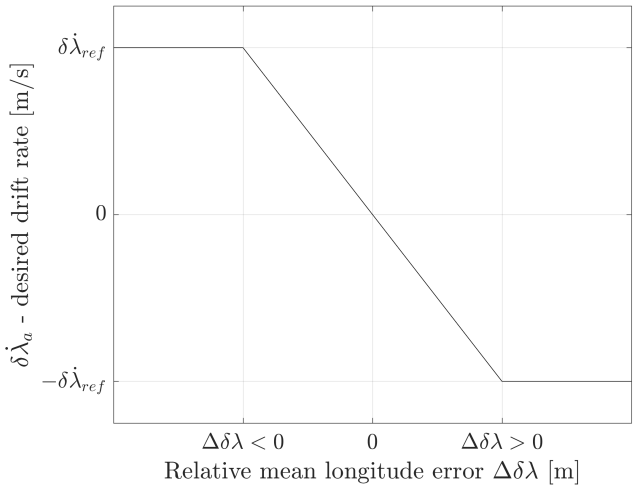

Figure 3: Desired drift rate of the relative mean longitude $\delta\lambda$.

A function that ensures this property and is centered at the desired reference $\delta\lambda_{\text{a}}$ is given by

$$\delta\dot{\lambda}_{\text{a}} = \begin{cases} -\min\left\{\frac{|\Delta\delta\lambda|}{\tau}, \delta\dot{\lambda}_{\text{ref}}\right\}, & \text{if } \Delta\delta\lambda \geq 0 \\ \min\left\{\frac{|\Delta\delta\lambda|}{\tau}, \delta\dot{\lambda}_{\text{ref}}\right\}, & \text{if } \Delta\delta\lambda < 0 \end{cases} \quad , \tag{15}$$

where $\tau \in \mathbb{R}^+$ is an arbitrary large scaling factor, which sets the amount of relative drift for a given error. The first case in Equation (15) is valid for a positive error of the relative mean longitude ($\Delta\delta\lambda \geq 0$). A negative drift is required to minimize the error. The second case is valid for a negative error of the relative mean longitude ($\Delta\delta\lambda < 0$), in which case a positive drift rate will minimize the error. The min-function ensures that the drift rate is limited to an upper bound for large errors of the relative mean longitude. The upper bound for the drift rate $\delta\dot{\lambda}_{\text{ref}}$ is given by

$$\delta\dot{\lambda}_{\text{ref}} = \frac{3}{2} n_c |\delta a_{\text{ref}}| \quad . \tag{16}$$

In order to derive δa_{ref}, it is important to understand that tangential thrust required for reconfiguring the relative eccentricity vector $\delta\boldsymbol{e}$ also affects the relative semi-major axis δa. The effect of a continuous tangential burn on the relative semi-major axis is given by the control input matrix $\boldsymbol{B}_c$ in Equation (4) by

$$\Delta\delta a_{\text{tan}} = \frac{2}{a_c n_c \eta_c}(1 + e_c \cos f_c) \cdot \Delta v_{\text{tan}} \quad , \tag{17}$$

where the velocity change Δv_{tan} is given by

$$\Delta v_{\text{tan}} = \frac{u_d \cdot T}{4} \prod_{q=N,N-2,\cdots}^{4} \frac{q-1}{q} \quad , \tag{18}$$

with the desired acceleration level u_d $\left[\mathrm{m/s^2}\right]$, orbit period T [s] and the exponent N as defined by the feedback gain matrix given by Equation (11). The desired relative semi-major axis δa_{ref} is set to half of $\Delta\delta a_{\text{tan}}$

$$|\delta a_{\text{ref}}| = \frac{|\Delta\delta a_{\text{tan}}|}{2} \quad . \tag{19}$$

By doing so, the actual relative semi-major axis, which oscillates about $|\delta a_{\text{ref}}|$ with an amplitude of $|\Delta\delta a_{\text{tan}}|$ due to tangential control inputs, will peak at $\delta a = 2|\delta a_{\text{ref}}|$ and dip at $\delta a = 0$ once per orbit. Thus, a change of the relative mean longitude into the desired direction is guaranteed. After $\delta\dot{\lambda}_{\text{a}}$ is determined using Equation (15), it has to be translated into a desired relative semi-major axis by applying Equation (14)

$$\delta a_a = -\frac{2}{3}\frac{\delta\dot{\lambda}_{\text{a}}}{n_c} \quad . \tag{20}$$

The desired relative semi-major axis δa_{a} is then applied to the controller for tracking and thus the mean along-track separation $\delta\lambda$ is indirectly controlled as well.

TRACKING THE RELATIVE SEMI-MAJOR AXIS WITH THE PROPOSED CONTROL STRATEGY

The in-plane motion of the relative geometry is defined by the relative eccentricity vector $\delta\boldsymbol{e}$ and the relative semi-major axis δa. The control input matrix, given by the Gauss' variational equations, shows that $\delta\boldsymbol{e}$ and δa are coupled such that control efforts to stabilize either $\delta\boldsymbol{e}$ or δa could possibly destabilize the other. The required direction of a tangential burn for controlling a given error of the relative eccentricity vector changes by 180° every half an orbit. The required tangential burn for a given relative semi-major axis error does not change its direction. This conflict of interest is illustrated in Figure 4.

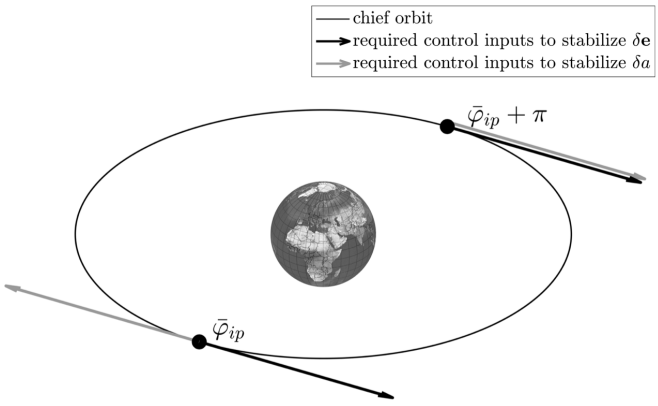

Figure 4: Absolute chief orbit with fuel optimal locations to apply tangential thrust for in-plane reconfigurations, $\varphi = \bar{\varphi}_{ip}$ and $\varphi = \bar{\varphi}_{ip} + \pi$.

Assuming desired changes in the relative semi-major axis are much smaller than in the relative eccentricity vector, which is true for bounded formations, this problem can be solved by defining a limit for the tracking error of the relative semi-major axis to be

$$|\Delta\delta a^{\text{max}}| = \frac{|\Delta\delta a_{\text{tan}}|}{2} \quad , \tag{21}$$

which is half the change of the relative semi-major axis due to one tangential burn. Therefore, the error of δa will always be $\Delta\delta a = \pm\frac{\Delta\delta a_{\text{tan}}}{2}$ at the beginning of a tangential burn and $\Delta\delta a = \mp\frac{|\Delta\delta a_{\text{tan}}|}{2}$ at the end of a tangential burn. Thus, an oscillation of δa about the desired reference δa_a is yielded. The maximum tracking error $|\Delta\delta a^{\max}|$ can be enforced by adjusting the feedback gain matrix $\boldsymbol{P}$ given in Equation (11) such that the error feedback is set to zero if the maximum error $|\Delta\delta a^{\max}|$ is violated

$$\boldsymbol{P}_{|\Delta\delta a|\geq|\Delta\delta a^{\max}|} = \frac{1}{k}\begin{pmatrix} 0 & 0 & 0 & 0 & 0 \\ 0 & 0 & 0 & 0 & 0 \\ 0 & 0 & 0 & 0 & 0 \\ 0 & 0 & 0 & \cos(H)^N & 0 \\ 0 & 0 & 0 & 0 & \cos(H)^N \end{pmatrix} \quad . \tag{22}$$

CONSTRAINTS

Time Constraint

Mission requirements usually impose time constraints on reconfigurations. The proposed control strategy allows to calculate the required thrust level in order to achieve a desired reconfiguration with a given optimal delta-v change. The feedback gain matrix in Equation (11) defines the shape of the applied control inputs (see Figure 2). The control inputs are characterized by a cosine shape centered at the fuel-optimal location with the even and positive exponent N. The delta-v change $\Delta v_{2\pi}$ for one orbit period of such continuous control accelerations is given by

$$\Delta v_{2\pi} = u_d \int_{\varphi=0}^{\varphi=2\pi} \cos(\varphi)^N \mathrm{d}\varphi \quad , \tag{23}$$

with u_d being the desired control acceleration and φ the mean argument of latitude. This integral can be solved using the reduction formula, which is given by

$$\int \cos(\varphi)^N \mathrm{d}\varphi = \frac{\sin(\varphi)\cos(\varphi)^{N-1}}{N} + \frac{N-1}{N}\int \cos(\varphi)^{N-2}\mathrm{d}\varphi \quad . \tag{24}$$

Note that N is defined to be an even number. Therefore, the term $\frac{1}{N}\sin(\varphi)\cos(\varphi)^{N-1}$, with an odd exponent for the cosine, can always be expressed in terms of $\sin(d\cdot\varphi)$ with d being an even number. An example for $N = 4$ is

$$\begin{aligned} \frac{1}{4}\sin(\varphi)\cos(\varphi)^3 &= \frac{1}{4}\left[\sin(\varphi)\cos(\varphi)\cdot\cos(\varphi)^2\right] \quad , \\ &= \frac{1}{4}\left[\frac{1}{2}\sin(2\varphi)\cdot\left(\frac{1}{2}+\frac{1}{2}\cos(2\varphi)\right)\right] \quad , \\ &= \frac{1}{16}\sin(2\varphi) + \frac{1}{16}\sin(2\varphi)\cos(2\varphi) \quad , \\ &= \frac{1}{16}\sin(2\varphi) + \frac{1}{32}\sin(4\varphi) \quad . \end{aligned} \tag{25}$$

For the integration from 0 to 2π Equation (25) becomes zero. Since $\sin(\varphi)\cos(\varphi)^{N-1}$ only has odd exponents as in the previous example, the first summand of Equation (24) is always zero and can be neglected. Equation (24) is rewritten as

$$\int_0^{2\pi} \cos(\varphi)^N \mathrm{d}\varphi = \frac{N-1}{N}\int_0^{2\pi} \cos(\varphi)^{N-2}\mathrm{d}\varphi \quad . \tag{26}$$

One can easily see that this reduction formula can be applied sequentially until the exponent $N-2$ is reduced to $N-2=2$, which is given for $N=4$. This product sequence is given by

$$\Delta v_{2\pi} = u_d \prod_{q=N,N-2,\cdots}^{4} \left[\frac{q-1}{q}\right] \cdot \int_0^{2\pi} \cos(\varphi)^2 \mathrm{d}\varphi \quad \text{, which can be rewritten as}$$

$$\Delta v_{2\pi} = u_d \prod_{q=N,N-2,\cdots}^{4} \left[\frac{q-1}{q}\right] \cdot \int_0^{2\pi} \frac{1}{2} + \frac{1}{2}\cos(2\varphi)\mathrm{d}\varphi \quad \text{, substitute } x = 2\varphi \text{ and } \frac{\mathrm{d}x}{\mathrm{d}\varphi} = 2$$

$$\Delta v_{2\pi} = u_d \prod_{q=N,N-2,\cdots}^{4} \left[\frac{q-1}{q}\right] \cdot \left(\frac{1}{2}\varphi\Big|_0^{2\pi} + \frac{1}{2}\int_0^{2\pi} \cos(x)\frac{\mathrm{d}x}{2}\right) \quad \text{, adjust integration boundaries}$$

$$\Delta v_{2\pi} = u_d \prod_{q=N,N-2,\cdots}^{4} \left[\frac{q-1}{q}\right] \cdot \left(\pi + \frac{1}{4}\sin(x)\Big|_0^{4\pi}\right) \quad \text{, resubstitute } x = 2\varphi$$

$$\Delta v_{2\pi} = u_d \prod_{q=N,N-2,\cdots}^{4} \left[\frac{q-1}{q}\right] \cdot \left(\pi + \frac{1}{4}\sin(2\varphi)\Big|_0^{2\pi}\right) \quad \text{, simplify}$$

$$\Delta v_{2\pi} = u_d\pi \cdot \prod_{q=N,N-2,\cdots}^{4} \frac{q-1}{q} \quad \left[\left(\frac{\mathrm{m}}{\mathrm{s}^2}\cdot \mathrm{rad}\right)\Big/\mathrm{orbit}\right] \quad \text{, multiply with } \frac{T}{2\pi}$$

$$\Delta v_{2\pi} = \frac{1}{2}u_d T \cdot \prod_{q=N,N-2,\cdots}^{4} \frac{q-1}{q} \quad \left[\left(\frac{\mathrm{m}}{\mathrm{s}}\right)\Big/\mathrm{orbit}\right] \quad , \tag{27}$$

where T is the chief's orbit period. The required optimal total in-plane $\Delta v_{ip}^{\text{opt}}$ and out-of-plane Δv_{oop}^{opt} velocity changes are given by

$$\Delta v_{ip}^{\text{opt}} = a_c n_c \cdot \frac{\|\Delta\delta\boldsymbol{e}\|}{2\eta_c} \quad \text{, see Chernick et al.}^{11}, \tag{28}$$

$$\Delta v_{oop}^{\text{opt}} = a_c n_c \frac{1-e_c}{\eta_c}\|\Delta\delta\boldsymbol{i}\| \quad . \tag{29}$$

In order for Equation (28) to hold true it is important that $\frac{\Delta\delta a}{2(1+e_c)}$ is smaller than $\frac{\|\Delta\delta\boldsymbol{e}\|}{2\eta^2}$. For reconfigurations from one bounded formation to another bounded formation this restriction is always satisfied. The applied velocity increment $\Delta v_{2\pi}$ has to be equal to the velocity change that is required during one orbit period $\frac{\Delta v^{\text{opt}}}{\#\text{ orbits}}$

$$\frac{\Delta v^{\text{opt}}}{\#\text{ orbits}} = \frac{1}{2}u_d T \cdot \left(\prod_{q=N,N-2,\cdots}^{4} \frac{q-1}{q}\right) \quad , \tag{30}$$

with the only unknown being u_d. Solving for the desired thrust levels into the orbit normal $u_{d,oop}$ and the orbit tangential direction $u_{d,ip}$ yields

$$u_{d,ip} = \frac{2\Delta v_{ip}^{\text{opt}}}{T\cdot\#\text{orbits}} \prod_{q=N,N-2,\cdots}^{4} \frac{q}{q-1} \quad \left[\frac{\mathrm{m}}{\mathrm{s}^2}\right] \quad , \tag{31}$$

$$u_{d,oop} = \frac{2\Delta v_{oop}^{\text{opt}}}{T\cdot\#\text{orbits}} \prod_{q=N,N-2,\cdots}^{4} \frac{q}{q-1} \quad \left[\frac{\mathrm{m}}{\mathrm{s}^2}\right] \quad . \tag{32}$$

Ensure that the thrusters also need to be capable of producing the desired control acceleration u_d. Furthermore, since the along-track separation is only indirectly controlled by leveraging Keplerian dynamics the maximum error in the along-track direction $|\Delta\delta\lambda|$ has to be smaller than

$$|\Delta\delta\lambda| \leq \frac{3}{2} n |\delta a_a| \cdot \#\text{orbits} \cdot T \quad . \tag{33}$$

Thrust Constraint

For low-thrust propulsion systems it is important that the thrusters are not continuously operated in saturation. Therefore a thrust constraint is formulated that ensures that a user defined thrust level is not exceeded by the control law. Note that the time constraint and the thrust constraint are mutually exclusive. The thrust constraint is given by

$$\|\boldsymbol{F}\| \leq F_{\text{desired}} \quad , \tag{34}$$

where F_{desired} has to be within the thruster levels, but larger than the relative dynamic perturbations such that a reconfiguration or formation maintenance is still possible.

Wall Constraints

Wall constraints restrict state-space variables to be always smaller or always greater than a defined threshold d_i. Those constraints can be formulated using[15]

$$\boldsymbol{c}_i^{\mathrm{T}} \delta\boldsymbol{\alpha} \leq d_i \quad , \tag{35}$$

$$\boldsymbol{c}_i^{\mathrm{T}} \delta\boldsymbol{\alpha} \geq d_i \quad , \tag{36}$$

with $\boldsymbol{c}_i \in \mathbb{N}^{5x1}$ and $d_i \in \mathbb{R}^+$. The parameter $\boldsymbol{c}_i$ defines the ROE vector element to be constrained with all elements being zero but one element which corresponds to the constrained element is 1. An example for constraining δi_x is given by

$$\boldsymbol{c} = \begin{pmatrix} 0 & 0 & 0 & 1 & 0 \end{pmatrix}^{\mathrm{T}}, \tag{37}$$

such that $\boldsymbol{c}^{\mathrm{T}} \delta\boldsymbol{\alpha} = \delta i_x$.

Circular No-Entry-Zone Constraint

A circular boundary of radius $r_i \in \mathbb{R}$, centered at $\boldsymbol{x}_i \in \mathbb{R}^2$ for any combination of two ROE can be formulated using

$$\|\boldsymbol{G}_i^{\mathrm{T}} \delta\boldsymbol{\alpha} - \boldsymbol{x}_i\| \geq r_i \quad , \tag{38}$$

with $\boldsymbol{G}_i \in \mathbb{N}^{5x2}$ and $r_i > 0$. The parameter $\boldsymbol{G}_i$ defines the ROE vector elements to be constrained with all elements being zero but two elements which correspond to the constrained elements being 1. For example, in order to constrain the relative eccentricity vector $\delta\boldsymbol{e}$ one has to define

$$\boldsymbol{G} = \begin{pmatrix} 0 & 1 & 0 & 0 & 0 \\ 0 & 0 & 1 & 0 & 0 \end{pmatrix}^{\mathrm{T}}, \tag{39}$$

such that $\boldsymbol{G}^{\mathrm{T}} \delta\boldsymbol{\alpha} = \delta\boldsymbol{e}$.

Passive Collision Avoidance

For satellite formations it is convenient to acquire passive collision safety by defining a safety distance ε in the rn-plane of the **RTN** frame as shown by the e-/i- vector separation algorithm by D'Amico and Montenbruck[18]

$$\delta r_{rn}^{\min} \geq \varepsilon \quad . \tag{40}$$

If this relative distance in the rn-plane is always guaranteed, no collisions can occur even in the presence of uncertainties in the mean along-track direction. The e-/i- vector separation algorithm is applicable for bounded motion.

REFERENCE GOVERNOR

This section deals with the guidance of the applied reference $\delta\boldsymbol{\alpha}_a$, at which the Lyapunov controller stabilizes the relative state, in order to satisfy the constraints imposed on the reconfiguration and to satisfy the complete set of end conditions. A reference governor (RG) that will guide the applied reference $\delta\boldsymbol{\alpha}_a$ through the ROE state-space while ensuring the satisfaction of the constraint set is developed. The RG uses an attractive potential field that is directed to the desired reference $\delta\boldsymbol{\alpha}_r$ and the constraints are realized by repulsive potential functions. Together, both the repulsive and the attractive fields compose a potential field map ϕ with gradient $\boldsymbol{\rho}$ at the current applied reference $\delta\boldsymbol{\alpha}_a$. Thus, the ROE state is guided along this gradient to the desired reference without violating any constraints. Following the potential field gradient $\boldsymbol{\rho}$ ensures that the steady state error is minimum without violating the constraint set. The rate of change $|\delta\dot{\boldsymbol{\alpha}}_a|$ at which the applied reference is guided, is controlled by formulating a Lyapunov threshold Γ for the Lyapunov function given by Equation (9). The Lyapunov threshold represents a maximum allowed tracking error since the Lyapunov value $V = 0.5\Delta\delta\boldsymbol{\alpha}_a^{\mathrm{T}}\Delta\delta\boldsymbol{\alpha}_a$ is a function of the tracking error itself. A Lyapunov threshold Γ_i is derived for each constraint that is imposed on the relative satellite state and the most restrictive Lyapunov threshold

$$\Gamma = \min\{\Gamma_i\} \tag{41}$$

is to be enforced by the RG.[16] Note that the derived Lyapunov thresholds Γ_i are suited for the specific Lyapunov function in use and change if a different Lyapunov function is used. All Γ_i are derived in the following sections. If the Lyapunov value V is smaller than its threshold Γ, all constraints are satisfied. Thus all constraints are translated into a single constraint by

$$V \leq \Gamma \quad , \tag{42}$$

which can be enforced using[15]

$$\delta\dot{\boldsymbol{\alpha}}_a = \xi\,[\Gamma - V]\cdot\boldsymbol{\rho} \quad , \tag{43}$$

where $\xi \in \mathbb{R}^+$ is an arbitrary large scalar. Equation (43) is the central equation of the RG. If the Lyapunov value V gets close to the Lyapunov threshold, the change of the applied reference tends to zero, because of $\lim_{V\to\Gamma}[\Gamma - V] = 0$, giving the system time to converge to the applied reference. If the ROE state is exactly at the applied reference $V = 0$ the change of the applied reference is maximized such that $\delta\boldsymbol{\alpha}_a$ reaches $\delta\boldsymbol{\alpha}_{\mathrm{r}}$ as quickly as possible. The gradient of ϕ is given by[16]

$$\boldsymbol{\rho} = \boldsymbol{\nabla}\phi \quad . \tag{44}$$

The operator $\boldsymbol{\nabla}(.)$ denotes taking the partial derivatives with respect to the applied reference $\delta\boldsymbol{\alpha}_a$ as

$$\boldsymbol{\nabla} = \left(\frac{\partial}{\partial\delta a}, \frac{\partial}{\partial\delta e_x}, \frac{\partial}{\partial\delta e_y}, \frac{\partial}{\partial\delta i_x}, \frac{\partial}{\partial\delta i_y}\right)_a \quad .$$

The gradient is a conservative function that tends to zero at $\delta\boldsymbol{\alpha}_a = \delta\boldsymbol{\alpha}_r$ and goes to infinity at the constraint boundaries. Since the sum of conservative functions is also conservative, $\boldsymbol{\rho}$ can be constructed by taking into account separate terms for each defined constraint.[16] After all potential field gradients are found, the vector field $\boldsymbol{\rho}$ is given by

$$\boldsymbol{\rho} = -\boldsymbol{\nabla}\bar{\phi} - \sum_{i=1}^{M} \boldsymbol{\nabla}\phi_i \quad , \tag{45}$$

where $\bar{\phi}$ is the global attractive potential field and ϕ_i are the repulsive potential fields of the constraints. M is the number of defined constraints.

Potential Field Map

The global attractive potential function is given by[16]

$$\bar{\phi} = \begin{cases} \|\delta\boldsymbol{\alpha}_a - \delta\boldsymbol{\alpha}_r\|, & \text{if } \|\delta\boldsymbol{\alpha}_a - \delta\boldsymbol{\alpha}_r\| \geq \eta \\ \frac{1}{2}\frac{\|\delta\boldsymbol{\alpha}_a - \delta\boldsymbol{\alpha}_r\|^2}{\eta} + \frac{1}{2}\eta, & \text{otherwise} \end{cases} \quad , \tag{46}$$

where $\eta \geq 1$ and $\eta \in \mathbb{R}$ is an arbitrary small user defined number. The gradient of the global potential field is given by

$$\boldsymbol{\nabla}\bar{\phi} = \frac{\delta\boldsymbol{\alpha}_a - \delta\boldsymbol{\alpha}_r}{\max\{\|\delta\boldsymbol{\alpha}_a - \delta\boldsymbol{\alpha}_r\|, \eta\}}, \tag{47}$$

which is unitary if $\|\delta\boldsymbol{\alpha}_a - \delta\boldsymbol{\alpha}_r\| \geq \eta$ and tends to zero for $\|\delta\boldsymbol{\alpha}_a - \delta\boldsymbol{\alpha}_r\| < \eta$. The parameter η is defined such that the gradient tends to zero for very small tracking errors with respect to the desired reference $\delta\boldsymbol{\alpha}_r$. Otherwise the applied reference $\delta\boldsymbol{\alpha}_a$ would not converge to the desired reference. A potential function for the constraints is given by[16]

$$\phi_i = \begin{cases} \frac{-\Upsilon_i^2(\zeta_i - C_i)^2}{(\zeta_i^2 - \Upsilon_i^2)C_i}, & \text{if } C_i \leq \zeta_i \\ 0, & \text{otherwise} \end{cases} \quad , \tag{48}$$

where C_i is the current distance of the applied reference $\delta\boldsymbol{\alpha}_a$ to the boundary of constraint i ,$\Upsilon_i \in \mathbb{R}^+$ is the safety margin and $\zeta_i \in \mathbb{R}^+$ is the influence distance, where $\zeta_i > \Upsilon_i$. For any $C_i > \zeta_i$, the constraint i does neither contribute to the potential field ϕ nor to the Lyapunov threshold given by Equation (70). The gradients for the two wall constraints are given by

$$\boldsymbol{\nabla}\phi_i = \begin{cases} \frac{\Upsilon_i^2(\zeta_i^2 - C_i^2)}{(\zeta_i^2 - \Upsilon_i^2)C_i^2}\boldsymbol{c}_i & \text{for constraint (35): } \boldsymbol{c}_i^{\mathrm{T}}\delta\boldsymbol{\alpha} \leq d_i \\ \frac{-\Upsilon_i^2(\zeta_i^2 - C_i^2)}{(\zeta_i^2 - \Upsilon_i^2)C_i^2}\boldsymbol{c}_i & \text{for constraint (36): } \boldsymbol{c}_i^{\mathrm{T}}\delta\boldsymbol{\alpha} \geq d_i \end{cases} \quad , \tag{49}$$

where $\boldsymbol{c}_i$ is defined by Equations (35) and (36). The gradient of the potential field of the circular no-entry-zone constraint is

$$\boldsymbol{\nabla}\phi_i = \frac{-\Upsilon_i^2(\zeta_i^2 - C_i^2)}{(\zeta_i^2 - \Upsilon_i^2)C_i^2}\frac{\boldsymbol{G}_i\left(\boldsymbol{G}_i^{\mathrm{T}}\delta\boldsymbol{\alpha} - \boldsymbol{x}_i\right)}{\|\boldsymbol{G}_i\delta\boldsymbol{\alpha} - \boldsymbol{x}_i\|} \quad , \tag{50}$$

where the parameters $\boldsymbol{G}_i$ and $\boldsymbol{x}_i$ are defined in Equation (38). The collision safety constraint is enforced by establishing a mean along-track separation if no passive safety in the rn-plane is given.

In order to guarantee a minimum spacecraft approach of the distance ε in the rn-plane the following three conditions have to be satisfied[13]

$$\|\delta \boldsymbol{e}\| \geq \varepsilon \quad , \tag{51}$$

$$\|\delta \boldsymbol{i}\| \geq \varepsilon \quad , \tag{52}$$

$$\|\delta \boldsymbol{e} \cdot \delta \boldsymbol{i}\| \geq \varepsilon \sqrt{\delta e^2 + \delta i^2 - \varepsilon^2} \quad . \tag{53}$$

A potential function for the passive collision avoidance constraint is defined by

$$\phi_{\text{rn}} = \begin{cases} \frac{-\Upsilon_{\text{rn}}^2 (\zeta_{\text{rn}} - C_{\text{rn}})^2}{(\zeta_{\text{rn}}^2 - \Upsilon_{\text{rn}}^2) C_{\text{rn}}}, & \text{if } C_{\text{rn}} \leq \zeta_{\text{rn}} \text{ and } |\delta\lambda| < 2 \cdot \|\delta \boldsymbol{e}\| + \varepsilon \\ 0, & \text{otherwise} \end{cases} \quad , \tag{54}$$

where the margin to the constraint C_{rn} is found using Equations (51) to (53) and is given by

$$C_{\text{rn}} = \min \left\{ \|\delta \boldsymbol{e}\| - \varepsilon, \|\delta \boldsymbol{i}\| - \varepsilon, \|\delta \boldsymbol{e} \cdot \delta \boldsymbol{i}\| - \varepsilon \sqrt{\delta e^2 + \delta i^2 - \varepsilon^2} \right\} \quad . \tag{55}$$

The gradient of this potential function given in Equation (54) is defined to

$$\boldsymbol{\nabla} \phi_{\text{rn}} = \phi_{rn} \cdot \left(-\boldsymbol{\nabla} \bar{\phi} \right) \quad . \tag{56}$$

At the boundary, where the minimum relative distance throughout one orbit period is exactly the defined minimum $\delta r_{rn}^{\text{min}} = \varepsilon$, the potential of the constraint is unitary $\phi_{rn} = 1$. Thus, the guidance of the relative inclination vector $\delta \boldsymbol{i}$ and the eccentricity vector $\delta \boldsymbol{e}$ are brought to a stop by the negation of the global potential field $-\boldsymbol{\nabla} \bar{\phi}$ in Equation (56). Note that this has only an effect on $\delta \boldsymbol{i}$ and $\delta \boldsymbol{e}$, but not on δa. While $\phi_{rn} = 1$, the following along-track separation has to be established to guarantee collision safety

$$\delta\lambda_{\text{safe}} = \begin{cases} 2 \cdot \|\delta \boldsymbol{e}\| + \varepsilon, & \text{if } C_{\text{rn}} \leq \zeta_{\text{rn}} \text{ and } |\delta\lambda| < 2 \cdot \|\delta \boldsymbol{e}\| + \varepsilon \text{ and } \delta\lambda > 0 \\ -2 \cdot \|\delta \boldsymbol{e}\| - \varepsilon, & \text{if } C_{\text{rn}} \leq \zeta_{\text{rn}} \text{ and } |\delta\lambda| < 2 \cdot \|\delta \boldsymbol{e}\| + \varepsilon \text{ and } \delta\lambda \leq 0 \end{cases} \quad , \tag{57}$$

which distinguishes the two cases $\delta\lambda > 0$ and $\delta\lambda \leq 0$. As soon as the constraint margin becomes smaller than the influence region ($C_{rn} \leq \zeta_{rn}$) the desired along-track separation $\delta\lambda_r$ has to be redefined to

$$\delta\lambda_r = \delta\lambda_{\text{safe}} \tag{58}$$

until passive collision safety is established again ($C_{rn} > \zeta_{rn}$). The time constraint and the thrust constraint both do not require a potential field in order to satisfy them. Both are enforced by using a Lyapunov threshold only as explained in the next section.

Lyapunov Threshold

The time constraint can be enforced without a potential field using only a Lyapunov threshold Γ_{thrust}. The applied control thrust is proportional to the tracking error $\Delta\delta\boldsymbol{\alpha}$ (see the control law in Equation (8)). Based on the current tracking error direction $\hat{\boldsymbol{\rho}}_e = \frac{\Delta\delta\boldsymbol{\alpha}}{\|\Delta\delta\boldsymbol{\alpha}\|}$, and assuming that this error direction is constant, one can calculate the control input $\hat{u}_c$ that is going to be applied by the controller per unit error in this direction

$$\hat{u}_c = \|\boldsymbol{B}^\star \boldsymbol{P} \hat{\boldsymbol{\rho}}_e\| \quad . \tag{59}$$

The tracking error into the direction of $\hat{\boldsymbol{\rho}}_e$ that is required in order to yield the desired control acceleration u_d can therefore be determined using Equation (59) and is given by

$$\|\Delta\delta\boldsymbol{\alpha}_{\text{req}}\| = \frac{u_d}{\hat{u}_c} \quad , \tag{60}$$

where u_d is defined by Equations (31) and (32). Equation (60) can easily be transferred into the Lyapunov form of Equation (9) to yield the Lyapunov threshold for the maximum thrust constraint by

$$\Gamma_{\text{time}} = \frac{1}{2}\|\Delta\delta\boldsymbol{\alpha}_{\text{req}}\|^2 = \frac{1}{2}\left(\frac{u_d}{\|\boldsymbol{B}^\star\boldsymbol{P}\hat{\boldsymbol{\rho}}_e\|}\right)^2 \quad . \tag{61}$$

The inverse of the control input matrix $\boldsymbol{B}^\star$ and the feedback gain matrix $\boldsymbol{P}$ are calculated at the delta-v optimal mean arguments of latitude for in-plane reconfigurations $\bar{\varphi}_{ip}$ and for out-of-plane reconfigurations $\bar{\varphi}_{oop}$. The Lyapunov threshold for the thrust constraint is derived the same way as the Lyapunov threshold for the time constraint in Equation (61). The only difference is that the desired control input is no longer a function of the desired reconfiguration, but a constant user defined value

$$\Gamma_{\text{thrust}} = \frac{1}{2}\left(\frac{F_{\text{desired}}/m_{sc}}{\|\boldsymbol{B}^\star\boldsymbol{P}\hat{\boldsymbol{\rho}}_e\|}\right)^2 \quad , \tag{62}$$

with m_{sc} being the spacecraft mass. It is important to note that the time and thrust constraints cannot be applied simultaneously. The Lyapunov threshold for the wall constraints can be found by using the margin of the constraint

$$C_i = |\boldsymbol{c}_i^{\mathrm{T}}\delta\boldsymbol{\alpha}_a - d_i| \quad , \tag{63}$$

where $\boldsymbol{c}_i$ and d_i are defined in Equations (35) and (36). Rewriting the margin C_i in Lyapunov form of Equation (9) yields

$$\Gamma_i = \frac{1}{2}C_i^2 = \frac{1}{2}(\boldsymbol{c}_i^{\mathrm{T}}\delta\boldsymbol{\alpha}_a - d_i)^2 \quad . \tag{64}$$

Similarly, the margin of the circular no-entry-zone is given by

$$C_i = \|\boldsymbol{G}_i^{\mathrm{T}}\delta\boldsymbol{\alpha}_a - \boldsymbol{x}_i\| - r_i \quad , \tag{65}$$

where $\boldsymbol{G}_i$, $\boldsymbol{x}_i$ and r_i are are defined in Equation (38). In analogy to Equation (64), the Lyapunov threshold for the circular no-entry-zone constraint (38) can be formulated by

$$\Gamma_i = \frac{1}{2}C_i^2 = \frac{1}{2}\left(\|\boldsymbol{G}_i^{\mathrm{T}}\delta\boldsymbol{\alpha}_a - \boldsymbol{x}_i\| - r_i\right)^2 \quad . \tag{66}$$

The Lyapunov threshold for the passive collision avoidance constraint is determined by first calculating the minimum cross-track separation given by D'Amico[10] for near-circular orbits with $\delta a = 0$

$$\delta r_{rn}^{\min} = \frac{\sqrt{2}|\delta\boldsymbol{e}\cdot\delta\boldsymbol{i}|}{\left(\delta e^2 + \delta i^2 + \|\delta\boldsymbol{e}+\delta\boldsymbol{i}\|\cdot\|\delta\boldsymbol{e}-\delta\boldsymbol{i}\|\right)^{1/2}} \quad . \tag{67}$$

The maximum allowable tracking error $\Delta\delta\boldsymbol{\alpha}_{\max}$ can be determined by performing a first order Taylor expansion of Equation (67) at the actual relative state $\delta\boldsymbol{\alpha}$ and is given by

$$\Delta\delta\boldsymbol{\alpha}_{\max} = \Delta\delta\boldsymbol{\alpha}\left(1 - \frac{\delta r_{rn}^{\min} - \varepsilon}{\left[0 \quad \frac{\partial\delta r_{rn}^{\min}}{\partial\delta e_x} \quad \frac{\partial\delta r_{rn}^{\min}}{\partial\delta e_y} \quad \frac{\partial\delta r_{rn}^{\min}}{\partial\delta i_x} \quad \frac{\partial\delta r_{rn}^{\min}}{\partial\delta i_y}\right]_{\delta\boldsymbol{\alpha}} \cdot \Delta\delta\boldsymbol{\alpha}_a}\right) \quad , \tag{68}$$

where the partial derivatives are given in Equations (76) to (79). The denominator in Equation (68) describes the unit change of $\delta r_{rn}^{\min}$ for an increase of the tracking error, while the numerator is the margin of the constraint (see the defintion of ε in Equation (40)). Therefore, the fraction describes how much the tracking error is allowed to become larger. It is noteworthy that an increase of the tracking error not always results in a smaller $\delta r_{rn}^{\min}$. Therefore, only if $\delta r_{rn}^{\min}$ decreases due to an increasing tracking error, Equation (68) is applicable to determine the Lyapunov threshold

$$\Gamma_{rn} = \begin{cases} \frac{1}{2}\Delta\delta\boldsymbol{\alpha}_{\max}^{\mathrm{T}}\Delta\delta\boldsymbol{\alpha}_{\max}, & \text{for } \begin{bmatrix} 0 & \frac{\partial\delta r_{rn}^{\min}}{\partial\delta e_x} & \frac{\partial\delta r_{rn}^{\min}}{\partial\delta e_y} & \frac{\partial\delta r_{rn}^{\min}}{\partial\delta i_x} & \frac{\partial\delta r_{rn}^{\min}}{\partial\delta i_y} \end{bmatrix}_{\delta\boldsymbol{\alpha}} \cdot \Delta\delta\boldsymbol{\alpha}_a < 0 \\ \infty, & \text{elsewhere} \end{cases} . \quad (69)$$

After all thresholds are found, the Lyapunov threshold that has to be enforced by the RG in Equation (43) is given by

$$\Gamma = \min\left\{\Gamma_{\text{time}}, \Gamma_{\text{thrust}}, \Gamma_i, \Gamma_{rn}\right\} \quad (70)$$

NUMERICAL VALIDATION

The guidance and control strategy is numerically validated using a high-fidelity orbit propagator named S^3, which includes orbit perturbations from atmospheric drag, high-order geopotential, solar radiation pressure and third-body (Moon and Sun) effects.[21] The true relative state positions and velocities are corrupted by realistic GPS sensor noise, that is then filtered by an Extended Kalman Filter. Control tracking errors are computed in mean ROE, while the propagator simulates each spacecraft individually in the Earth-centered inertial (ECI) coordinate frame. A conversion from ECI over osculating to mean orbit elements is performed in order to find the mean ROE. An actuator model represents a low-thrust Field Emission Electric Propulsion (nanoFEEP)system[2] that is currently being developed by the Universities of Würzburg and Dresden and is going to be used on the NetSat mission.

Example 1: Thrust Constraint and Optimality

This example shows a reconfiguration from an initial state-space configuration to a desired one with only a thrust constraint being imposed on the relative state. The thrust is restricted to peak at $10\,\mu\text{N}$. The initial configuration $a_c\delta\boldsymbol{\alpha}_0$ and the desired configuration $a_c\delta\boldsymbol{\alpha}_r$ are given as

$$a_c\delta\boldsymbol{\alpha}_0 = \begin{pmatrix} a_c\delta a \\ a_c\delta\lambda \\ a_c\delta e_x \\ a_c\delta e_y \\ a_c\delta i_x \\ a_c\delta i_y \end{pmatrix}_0 = \begin{pmatrix} 0 \\ 712 \\ 400 \\ 400 \\ 0 \\ 350 \end{pmatrix} \text{[m]} \quad , a_c\delta\boldsymbol{\alpha}_r = \begin{pmatrix} a_c\delta a \\ a_c\delta\lambda \\ a_c\delta e_x \\ a_c\delta e_y \\ a_c\delta i_x \\ a_c\delta i_y \end{pmatrix}_{\text{ref}} = \begin{pmatrix} 0 \\ 212 \\ 200 \\ 200 \\ 0 \\ 200 \end{pmatrix} \text{[m]} \quad . \quad (71)$$

The initial chief's classical orbit parameters are given as a near-circular low Earth retrograde polar orbit by

$$\boldsymbol{\alpha}_{c,0} = \begin{pmatrix} a_c \\ e_c \\ i_c \\ \Omega_c \\ \omega_c \\ M_c \end{pmatrix}_0 = \begin{pmatrix} 6892\,\text{km} \\ 0.0001384 \\ 97.400000^\circ \\ 266.153900^\circ \\ 89.119800^\circ \\ 45.880000^\circ \end{pmatrix} \quad . \quad (72)$$

The delta-v lower bound is derived with Equations (28) and (29) from the desired corrections $\Delta\delta\boldsymbol{e}$ and $\Delta\delta\boldsymbol{i}$ as

$$\Delta v_{lb} = \frac{a_c n_c}{\eta_c} \cdot \left(\frac{\|\Delta\delta\boldsymbol{e}\|}{2} + (1 - e_c)\|\Delta\delta\boldsymbol{i}\| \right) = 0.3206 \left[\frac{\mathrm{m}}{\mathrm{s}}\right] \quad . \tag{73}$$

Figure 5 shows the actual delta-v consumption of the full reconfiguration, which is given by $\Delta v = 0.3272$ [m/s]. This fuel consumption corresponds to a $2.1\,\%$ higher fuel consumption than the optimal delta-v lower bound Δv_{lb}. It is important to note that the lower bound was calculated without accounting for relative orbit perturbations. Furthermore, both spacecraft require about the same amount of delta-v which results in an equal fuel consumption. The deputy spacecraft requires $1.1\,\%$ more delta-v than the chief spacecraft. Figure 5 also shows the successful enforcement of the thrust constraint.

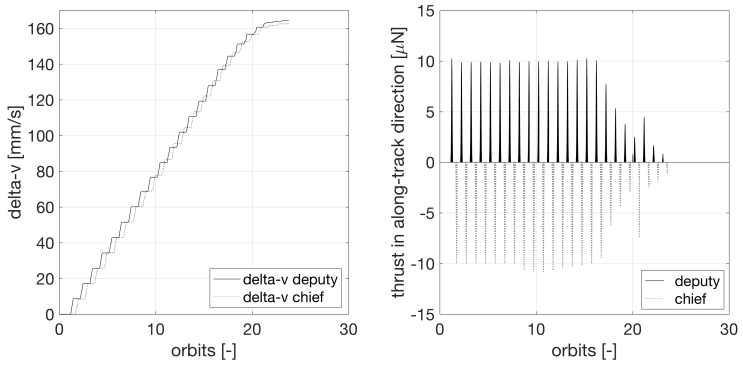

Figure 5: Reconfiguration example with imposed thrust constraint of $10\,\mu$N. Delta-v consumption (left) and control thrust inputs of the along-track thrusters (right).

Example 2: Time Constraint

In this example a reconfiguration is performed with an imposed time constraint of 25 orbits reconfiguration time. The initial and final relative states are the same as in the previous example. The time constraint can be enforced the same way as the thrust constraint. The difference is that the desired thrust level is calculated as a function of the remaining reconfiguration time and the desired reference. Therefore, the thrust constraint has to enforce the required thrust values as given by Equations (31) and (32). Figure 6 shows that all mean ROE errors are removed exactly at 25 orbits.

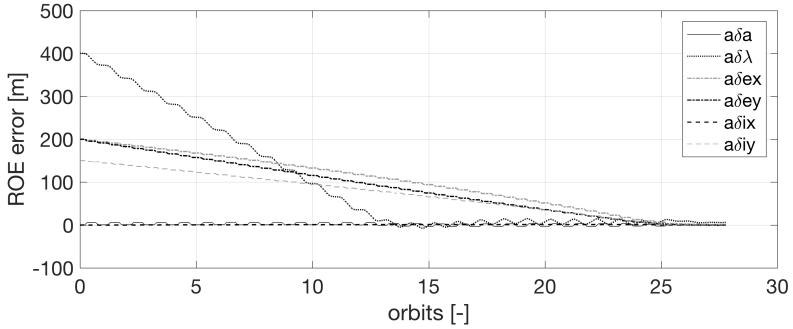

Figure 6: Reconfiguration example with imposed time constraint of 25 orbits.

Example 3: Wall Constraints

This example uses the same initial and desired relative states as the previous two examples, only the initial x-component of the inclination vector is changed to $\delta i_{x,0} = 100\,\text{m}$. Two wall constraints are imposed on the relative eccentricity/inclination vectors. The y-component of the inclination vector shall always be bigger than $\delta i_y \geq 250\,\text{m}$ and the x-component of the eccentricity vector shall always be bigger than $\delta e_x \geq 270\,\text{m}$. These constraints are formulated by

$$c_1^{\mathrm{T}} \delta\boldsymbol{\alpha} \geq d_1 \qquad \text{and} \qquad c_2^{\mathrm{T}} \delta\boldsymbol{\alpha} \geq d_2 \quad , \tag{74}$$

$$\begin{pmatrix} 0 & 0 & 0 & 0 & 1 \end{pmatrix}^{\mathrm{T}} \delta\boldsymbol{\alpha} \geq 250 \qquad \text{and} \qquad \begin{pmatrix} 0 & 1 & 0 & 0 & 0 \end{pmatrix}^{\mathrm{T}} \delta\boldsymbol{\alpha} \geq 270 \quad . \tag{75}$$

Both constraints are defined with an influence region of $\zeta = 50\,\text{m}$ and a safety distance of $\Upsilon = 10\,\text{m}$. Therefore, δi_y should not become smaller than $260\,\text{m}$ and δe_x should not become smaller than $280\,\text{m}$. Figure 7 shows the complete reconfiguration in ROE state-space. The x-axis represents the mean along-track separation $\delta\lambda$ and the x-components of the relative eccentricity/inclination vectors. The y-axis represents δa and the y-components of $\delta\boldsymbol{i}$ and $\delta\boldsymbol{e}$. One can see how at first both $\delta\boldsymbol{e}$ and $\delta\boldsymbol{i}$ approach the desired relative state without being affected by the constraints. Only $50\,\text{m}$ before the constraint boundary those constraints contribute to the potential field. They are deflected and become parallel to the constraint in order to minimize the steady-state error as intended.

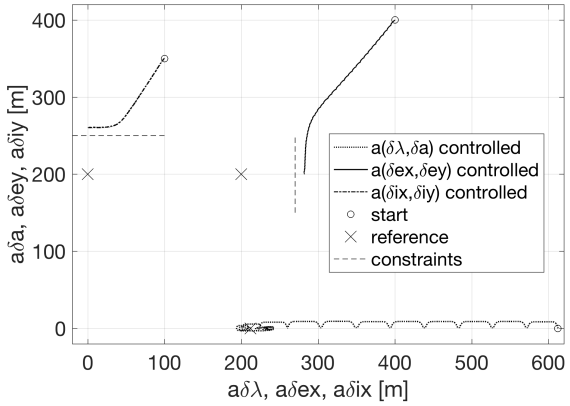

Figure 7: Reconfiguration example with two wall constraints on the inclination and eccentricity vectors.

CONCLUSIONS

Inspired by the NetSat formation-flying mission, this work addresses a strategy to perform a formation reconfiguration with respect to a chief satellite on closed orbits of arbitrary eccentricity through continuous low-thrust maneuvers. The employment of continuous thrust accelerations is prone to high delta-v consumption. Therefore this paper presents a continuous low-thrust guidance and control strategy, motivated by the attempt to spend the minimum possible delta-v. The relative dynamics are parameterized through relative orbit elements. These parameters provide descriptive insight into the characteristics of the relative satellite motion. It allowed to find a guidance and control algorithm which is able to satisfy the complete set of end conditions through orbit tangential

and orbit normal thrust accelerations only. The controller is a simple feedback design based on Lyapunov theory. It is enhanced by the development of an advanced feedback gain matrix, which centers the continuous maneuvers at the optimum locations in orbit. Furthermore, in order to minimize delta-v consumption, natural orbit dynamics are leveraged such that no radial thrust has to be applied. Special focus has been given to the determinism of a maneuvering scheme. This concerns the easiness of computing magnitudes and locations of the required maneuvers. Another relevant property is the predictability of the relative motion during a reconfiguration after each continuous thrust input. The chosen feedback gain matrix, which shapes the thrust profile, enables the control strategy to meet time constraints. Moreover, in addition to time constraints, reconfigurations can be performed while satisfying user-defined constraints on thrust magnitude and restricted state-space areas. Finally, the use of a reference governor revealed helpful to guide the spacecraft through the constrained state-space. Simple algorithms based on potential fields and the used Lyapunov function are formulated in ROE space to enforce relevant formation-flying constraints. Simulations have shown that the continuous control strategy performs near-optimal as compared to the delta-v optimized impulsive solution with an increase in delta-v consumption of under $4\,\%$. The discussed constraints can be enforced using the proposed reference governor.

Possible further work comprises the extension of this work to swarms of satellites. Problems will arise for the fuel balancing of all spacecraft involved in the swarm. Ideas in order to solve this problems are to assign pairs of spacecraft in a swarm formation that will apply the presented control strategy of this study and to find an autonomous on-board algorithm that is smart in finding a virtual center of the formation to which all other spacecraft pairs keep or reconfigure their states. This way it is possible to find a virtual center that ensures equal fuel consumption between already balanced spacecraft pairs. Furthermore, a repulsive potential field may be imposed on each spacecraft for active collision avoidance to move forward the passive collision approach. In the proposed control strategy only Keplerian dynamics are leveraged in order to achieve near-optimal delta-v consumption. The way forward is to leverage the differential J_2 effect as well if time constraints allow. The differential J_2 effect leads to a rotation of the relative eccentricity vector. This rotation can be used if it is helpful for a desired reconfiguration.

ACKNOWLEDGEMENTS

This study has been motivated by the NetSat mission and was realized at the Space Rendezvous Laboratory (SLAB) at Stanford University in a partnership by Stanford University, Zentrum für Telematik e.V. (ZfT) and the University of Würzburg (JMUW). The main author would like to thank Prof. Simone D'Amico, including his team at SLAB, for the support and the useful technical discussions. Furthermore, the author wants to express gratefulness to Prof. Klaus Schilling (JMUW, ZfT) for his trust and the given opportunities.

REFERENCES

[1] K. Schilling, P. Banger, P. Busch, S. Dombrovski, S. Freimann, A. Kleinschrodt, A. Kramer, T. Nogueira, D. Ris, J. Scharnagl, and T. Tzschichholz, "NETSAT: A Four Pico/Nano-Satellite Mission for Demonstration of Autonomous Formation Flying," 66th International Astronautical Congress, Jerusalem, Israel, October 12-16, 2015.

[2] D. Bock, A. Kramer, P. Bangert, K. Schilling, and M. Tajmar, "NanoFEEP on UWE platform Formation Flying of CubeSats using Miniaturized Field Emission Electric Propulsion Thrusters," Joint Conference of 30th ISTS, 34th IEPC and 6th NSAT, Kobe-Hyogo, Japan, July 6-10, 2015.

[3] H. Schaub, S. R. Vadali, J. L. Junkins, and K. T. Alfriend, "Spacecraft Formation Flying Control using Mean Orbit Elements," *AAS Journal of the Astronautical Sciences*, Vol. 48, No. 1, Jan.-March, 2000, pp. 69–87.

[4] H. Schaub and J. L. Junkins, *Analytical Mechanics of Space Systems*. AIAA Education Series, Reston, VA, 2003, DOI 10.2514/4.861550.

[5] M. Guelman and M. Aleshin, "Optimal Bounded Low-Thrust Rendezvous with Fixed Terminal-Approach Direction," *Journal of Guidance, Control, and Dynamics*, Vol. 24, No. 2, 2001, pp. 378–385, DOI 10.2514/2.4722.

[6] C. Lembeck and J. Prussing, "Optimal Impulsive Intercept with Low-Thrust Rendezvous Return," *Journal of Guidance, Control, and Dynamics*, Vol. 16, No. 3, 1993, pp. 426–433, DOI 10.2514/3.21027.

[7] T. E. Carter, "Optimal Power-Limited Rendezvous for Linearized Equations of Motion," *Journal of Guidance, Control, and Dynamics*, Vol. 17, No. 5, 1994, pp. 1082–1086, DOI 10.2514/3.21313.

[8] W. Dunbar and R. Murray, "Model predicitive control of coordinated multi-vehicle formations," *Proceedings of the 41st IEEE Conference on Decision and Control*, December 10-13, 2002, DOI 10.1109/CDC.2002.1185108.

[9] M. S. d. Queiroz, V. Kapila, and Q. Yan, "Adaptive Nonlinear Control of Multiple Spacecraft Formation Flying," *Journal of Guidance, Control, and Dynamics*, Vol. 23, No. 3, 2000, pp. 385–390, DOI 10.2514/2.4549.

[10] S. D'Amico, *Autonomous Formation Flying in Low Earth Orbit*. Ph.D. Thesis, Technical University of Delft, Delft, The Netherlands, March 2010.

[11] M. Chernick and S. D'Amico, "New Closed-Form Solutions for Optimal Impulsive Control of Spacecraft Relative Motion," *AIAA/AAS Astrodynamics Specialist Conference, AIAA SPACE Forum (AIAA 2016-5659)*, Long Beach, CA, Sept. 13-16, 2016, DOI 10.2514/6.2016-5659.

[12] G. Gaias, J.-S. Ardaens, and O. Montenbruck, "Model of J2 Perturbed Satellite Relative Motion with Time-Varying Differential Drag," *Celestial Mechanics and Dynamical Astronomy*, Vol. 123, No. 4, 2015, pp. 411–433, DOI 10.1007/s10569-015-9643-2.

[13] A. Koenig, T. Guffanti, and S. D'Amico, "New State Transition Matrices for Relative Motion of Spacecraft Formations in Perturbed Orbits," *AIAA/AAS Astrodynamics Specialist Conference, AIAA SPACE Forum, (AIAA 2016-5635)*, Long Beach, CA, Sept. 13-16, 2016, DOI 10.2514/6.2016-5635.

[14] L. Riggi and S. D'Amico, "Optimal Impulsive Closed-Form Control of Spacecraft Formation Flying and Rendezvous," American Control Conference (AAC), IEEE, Boston, MA, July 6-8, 2016, pp. 5854–5861, DOI 10.1109/ACC.2016.7526587.

[15] M. Nicotra, R. Naldi, and E. Garone, "A Robust Explicit Reference Governor for Constrained Control of Unmanned Aerial Vehicles," American Control Conference (ACC), IEEE, Boston, MA, July 6-8, 2016, pp. 6284–6289, DOI 10.1109/ACC.2016.7526657.

[16] M. Nicotra, M. Bartulovic, and E. Garone, "A Distributed Explicit Reference Governor for Constrained Control of Multiple UAVs," 5th IFAC Workshop on Distributed Estimation and Control in Networked Systems NecSys 2015, Philadelphia, PA, Sept. 10-11, 2015, pp. 156–161, DOI 10.1016/j.ifacol.2015.10.323.

[17] M. Nicotra and E. Garone, "Explicit Reference Governor for Constrained Nonlinear Systems," *IEEE Transactions on Automatic Control*, Vol. 61, May 2016, pp. 1379–1384, DOI 10.1109/TAC.2015.2476195.

[18] S. D'Amico and O. Montenbruck, "Proximity Operations of Formation Flying Spacecraft using an Eccentricity/Inclination Vector Separation," *Journal of Guidance, Control, and Dynamics*, Vol. 29, No. 3, 2006, pp. 554–563, DOI 10.2514/1.15114.

[19] G. Gaias and S. D'Amico, "Impulsive Maneuvers for Formation Reconfiguration Using Relative Orbital Elements," *Journal of Guidance, Control, and Dynamics*, Vol. 38, No. 6, 2015, pp. 1036–1049, DOI 10.2514/1.G000189.

[20] S. De Florio, S. D'Amico, and G. Radice, "Virtual Formation Method for Precise Autonomous Absolute Orbit Control," *Journal of Guidance, Navigation and Control*, Vol. 37, No. 2, 2014, pp. 425–438, DOI 10.2514/1.61575.

[21] D. Eddy, V. Giralo, and S. D'Amico, "Development and Verification of the Stanford GNSS Navigation Testbed for Spacecraft Formation-Flying," 9th International Workshop on Satellite Constellations and Formation Flight (IWSCFF), The University of Colorado Boulder, CO, June 19-21, 2017.

PARTIAL DERIVATIVES

$$\frac{\partial \delta r_{rn}^{\min}}{\partial \delta e_x} = \frac{a_c}{2\sqrt{2}} \left(\delta e^2 + \delta i^2 - \sqrt{\delta e^4 + \delta i^4 - 2\delta e^2 \delta i^2 \cos\left(2\left(\sigma - \theta\right)\right)} \right)^{-1/2} \Bigg[2\delta e_x - \frac{1}{2} \left(\delta e^4 + \delta i^4 - 2\delta e^2 \delta i^2 \cos\left(2\left(\sigma - \theta\right)\right) \right)^{-1/2} \Big(4\delta e^2 \delta e_x - 4\delta e_x \delta i^2 \cos\left(2\left(\sigma - \theta\right)\right) - 4\delta i^2 \delta e_y \sin\left(2\left(\sigma - \theta\right)\right) \Big) \Bigg] \tag{76}$$

$$\frac{\partial \delta r_{rn}^{\min}}{\partial \delta e_y} = \frac{a_c}{2\sqrt{2}} \left(\delta e^2 + \delta i^2 - \sqrt{\delta e^4 + \delta i^4 - 2\delta e^2 \delta i^2 \cos\left(2\left(\sigma - \theta\right)\right)} \right)^{-1/2} \Bigg[2\delta e_y - \frac{1}{2} \left(\delta e^4 + \delta i^4 - 2\delta e^2 \delta i^2 \cos\left(2\left(\sigma - \theta\right)\right) \right)^{-1/2} \Big(4\delta e^2 \delta e_y - 4\delta e_y \delta i^2 \cos\left(2\left(\sigma - \theta\right)\right) + 4\delta i^2 \delta e_x \sin\left(2\left(\sigma - \theta\right)\right) \Big) \Bigg] \tag{77}$$

$$\frac{\partial \delta r_{rn}^{\min}}{\partial \delta i_x} = \frac{a_c}{2\sqrt{2}} \left(\delta e^2 + \delta i^2 - \sqrt{\delta e^4 + \delta i^4 - 2\delta e^2 \delta i^2 \cos\left(2\left(\sigma - \theta\right)\right)} \right)^{-1/2} \Bigg[2\delta i_x - \frac{1}{2} \left(\delta e^4 + \delta i^4 - 2\delta e^2 \delta i^2 \cos\left(2\left(\sigma - \theta\right)\right) \right)^{-1/2} \Big(4\delta i^2 \delta i_x - 4\delta i_x \delta e^2 \cos\left(2\left(\sigma - \theta\right)\right) + 4\delta e^2 \delta i_y \sin\left(2\left(\sigma - \theta\right)\right) \Big) \Bigg] \tag{78}$$

$$\frac{\partial \delta r_{rn}^{\min}}{\partial \delta i_y} = \frac{a_c}{2\sqrt{2}} \left(\delta e^2 + \delta i^2 - \sqrt{\delta e^4 + \delta i^4 - 2\delta e^2 \delta i^2 \cos\left(2\left(\sigma - \theta\right)\right)} \right)^{-1/2} \Bigg[2\delta i_y - \frac{1}{2} \left(\delta e^4 + \delta i^4 - 2\delta e^2 \delta i^2 \cos\left(2\left(\sigma - \theta\right)\right) \right)^{-1/2} \Big(4\delta i^2 \delta i_y - 4\delta i_y \delta e^2 \cos\left(2\left(\sigma - \theta\right)\right) - 4\delta e^2 \delta i_x \sin\left(2\left(\sigma - \theta\right)\right) \Big) \Bigg] \tag{79}$$